LAWRENCE
LIVERMORE
NATIONAL
LABORATORY

LLNL-PROC-458080

Progress in the Development of Advanced Spherical Torus Operating Scenarios in NSTX.

S. P. Gerhardt, D. A. Gates, J. E. Menard, M. G. Bell, R. E. Bell, J. M. Canik, E. Fredrickson, S. Kaye, E. Kolemen, H. Kugel, B. P. Le Blanc, R. Maingi, D. Mastrovito, D. Mueller, S. A. Sabbagh, V. Soukhanovskii, H. Yuh

October 5, 2010

23rd IAEA Fusion Energy Conference
Daejon, South Korea
October 11, 2010 through October 16, 2010

Disclaimer

EXS/P2-08

Progress in the Development of Advanced Spherical Torus Operating Scenarios in NSTX.

S.P. Gerhardt 1), D. A Gates 1), J.E. Menard 1), M. G. Bell 1), R.E. Bell 1), J.M. Canik 2), E. Fredrickson 1), S. Kaye 1), E. Kolemen 1), H. Kugel 1), B. P. Le Blanc 1), R. Maingi 2), D. Mastrovito 1) D. Mueller 1), S. A. Sabbagh 3), V. Soukhanovskii 4), H. Yuh 5)

1) Princeton Plasma Physics Laboratory, Princeton NJ, 08543 USA
2) Oak Ridge National Laboratory, Oak Ridge TN, 37831 USA.
3) Columbia University, New York NY, 10027 USA
4) Nova Photonics, Princeton NJ, 08540 USA
5) Lawrence Livermore National Laboratory, Livermore CA, 94550 USA

E-mail contact of main author: sgerhard@pppl.gov

Abstract. Progress in the development of integrated advanced ST plasma scenarios in NSTX is reported. Recent high-performance plasmas in NSTX have operated at higher elongation and lower internal inductance than in previous years. Analysis during MHD-free periods has shown that the current profile can be understood as the sum of pressure driven, inductive, and neutral beam driven currents, without any anomalous fast ion transport. Non-inductive fractions of 65-70% have been routinely achieved in these configurations. A weaker B_T dependence of confinement is observed in these plasmas compared to previous studies, and the confinement is in general quite comparable to the expectations from higher-aspect ratio scalings. A β_N controller has been commissioned and utilized in high-performance plasmas. Some of these low-inductance discharges have a significantly reduced no-wall β_N limit, and often have β_N at or near the with-wall limit.

1. Introduction:

The spherical torus [1] has been suggested as the fusion core configuration for both fusion reactors and fusion technology development. As a reactor [2,3], the current drive power and TF dissipation must be minimized. The device would thus need to operate at simultaneously high elongation (κ) and normalized β [$\beta_N=\beta_T/(I_P/aB_T)$, in %mT/MA], since the product of the toroidal beta and pressure driven current fraction is proportional to $(1+\kappa^2)\beta_N^2$ [4,5]; typical values are κ~3.0-3.2 and β_N~8. As a device to study plasma material interactions [6] or nuclear technology [7-9] a substantial fraction (~50%) of the current can be provided by fast ions from injected neutral beams. This relaxes the equilibrium requirements somewhat, though high elongation (2.5-3) and β_N (3.5-4.5) are still required.

This paper describes plasmas in NSTX [10] designed to study the characteristics of sustained, high-elongation, high–β scenarios. Section 2 presents a few example discharges, while Section 3 presents analysis of the current profile and non-inductive fraction. The transport properties of these

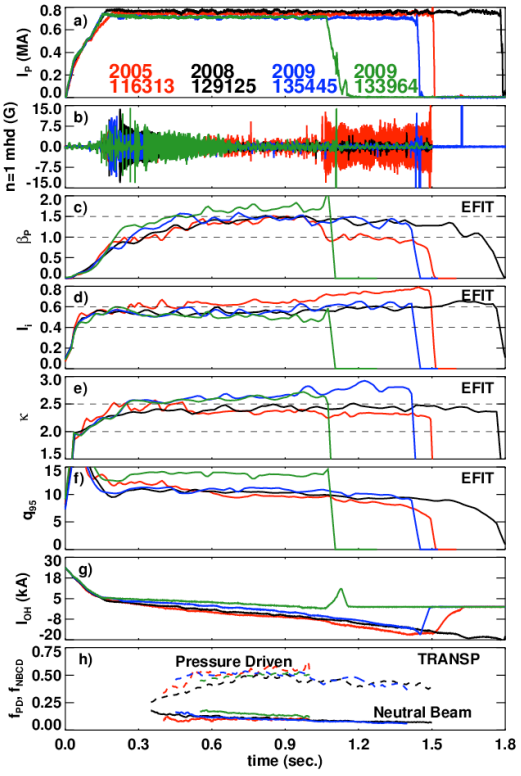

Fig. 1) Characteristics of discharges designed to optimize the non-inductive fraction and pulse duration.

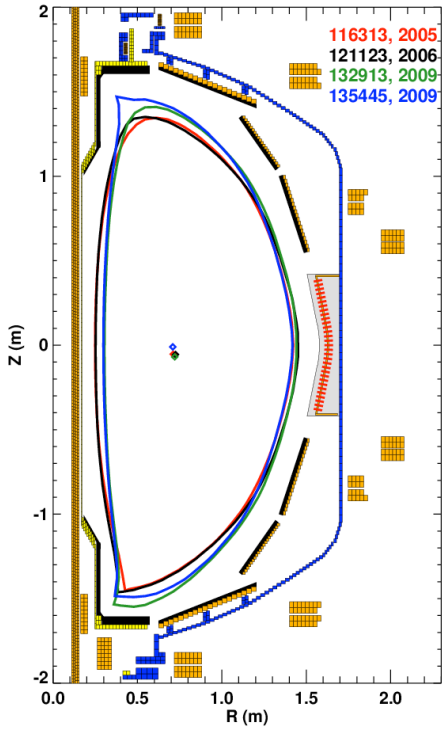

Fig. 2. Plasma boundary shapes for discharges studied in this paper.

plasmas are briefly described in Section. 4, and a discussion regarding magnetohydrodynamic (MHD) stability and control is given in Section 5.

2. Example Discharges at the NSTX Performance Boundary

Fig. 1 shows time traces from discharges designed to operate with maximum pulse length or highest β_P. These are slightly different optimization targets because the large toroidal field that maximizes β_P is inconsistent with long pulse due to TF coil heating limits. Here, β_P is defined as $\beta_P = 2\mu_0\langle P\rangle_{Vol}/B_P^2$ with $B_P = \mu_0 I_P/l_{pol}$ with l_{pol} the poloidal circumference of the separatrix. Discharge 116313 (red), from 2005 and before the advent of error field correction or lithium PFC conditioning, had an NSTX-best pulse length and sustained non-inductive fraction at the time, but succumbed to an m/n=1/1 rotating MHD mode midway through the discharge [11]. The lower single null shape of this plasma is shown in red in Fig. 2. Discharge 129125 (black), from 2008, is the longest pulse to date in NSTX, lasting ~300 ms. past the ramp-down of the toroidal field [12]. This discharge maintains a high-β state through the pulse, with no core-MHD. The use of error-field control and lithium conditioning was critical in achieving this state. The final two discharges are from the 2009 campaign, and have slightly lower current (700 vs. 750 kA). Discharge 133964 (green) is also operated at increased toroidal field (B_T=0.48 T instead of 0.38); see Ref. [13] for the first discussion of this discharge class. These recent discharges differ from earlier examples by their higher elongation (~2.6 compared to 2.3. see Fig. 2) and lower internal inductance l_i. Discharge 133964 in particular has a surface-average loop voltage of 130mV, the lowest ever achieved in a beam-heated H-mode in NSTX; it also has the highest flat-top average β_P. Considering the non-inductive fractions in the lowest frame, we see that 133964 has a neutral beam current drive fraction of ~18% in the early lower-density phase, significantly exceeding that from previous discharges. The bootstrap fraction reliably exceeds 50% in these scenarios. The confinement is comparable to or better than that expected from ITER-98 H-mode scaling [14].

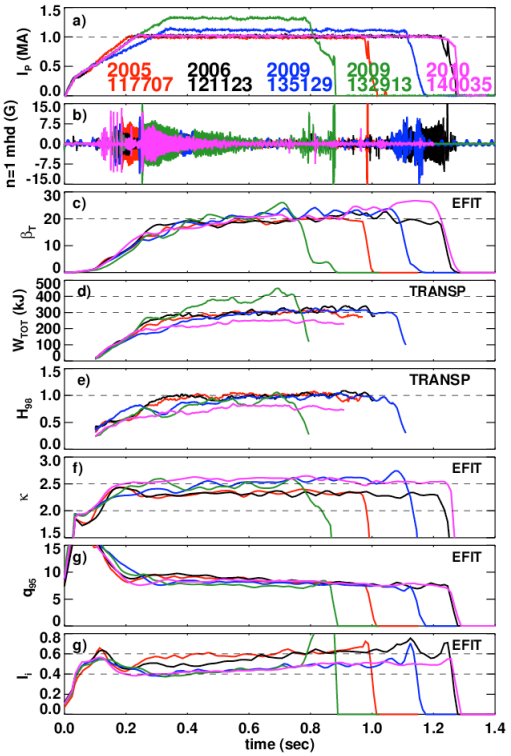

Fig. 3. Characteristics of discharges designed to optimize the stored energy and toroidal β.

The second style of discharge optimization, illustrated in Fig. 3, is to increase the toroidal beta and/or the stored energy. An extreme version of is shown in the I_P=1300 kA, B_T= 0.49 T discharge 132913 (green), which set the present NSTX stored

energy record of 460 kJ; this discharge was taken soon after lithium conditioning began in 2008, and clearly benefited from the improved confinement that lithium PFC conditioning provides. A single 1100 kA discharge from 2009 (135129 in blue), and a series of 1 MA discharges (117707 from 2005 in red, 121123 from 2006 in black, and 140035 from 2010 in magenta) are also shown. Inspection of the figure shows that the most recent discharges maintain a comparable or higher beta value, with high-elongation and lower l_i. In particular, the most recent 1 MA pulses (like 140035) are able to avoid the onset of any n=1 rotating modes for the duration of the pulse. The confinement is comparable to ITER-98 H-mode scaling in all cases.

The discussion of example discharges above shows that it has been difficult to achieve large increases in sustained β_T or non-inductive fraction (f_{NI}), compared to previous best shots from the 2005-2007 campaigns. Significant progress has been made, however, in developing the high-elongation scenarios and operating at reduced internal inductance. Furthermore, the reliability of these scenarios, as assessed by the duration of sustained high-β and the shot-to-shot reproducibility, has improved dramatically.

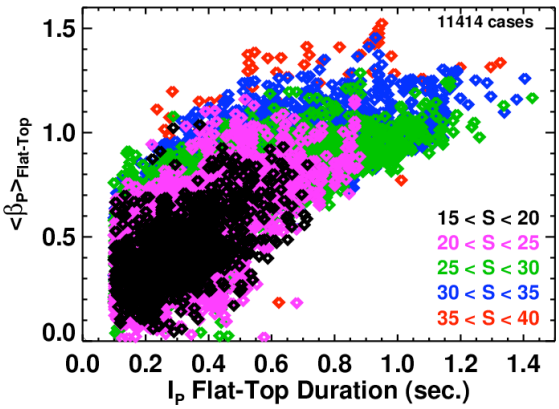

Fig. 4) β_P, averaged over the I_P flat-top, plotted against the I_P flat-top duration.

3. Current Profile Analysis and the Non-Inductive Fraction in NSTX

We have noted above that high-performance plasmas in NSTX have relied on plasmas shaping [15]. This plasma shape can be captured by the shape parameter $S = q_{95} I_P / aB_T$ [16], which increases with both elongation and triangularity. Figure 4 shows pulse average beta poloidal as a function of the I_P flat-top duration, for the vast majority of discharges in the NSTX database. It is clear that high values of shape factor facilitate high-performance operation, both by increasing the value of q for fixed I_P and B_T, and, through the triangularity, increasing the faction of the field line length that is spent in the good curvature high toroidal field region.

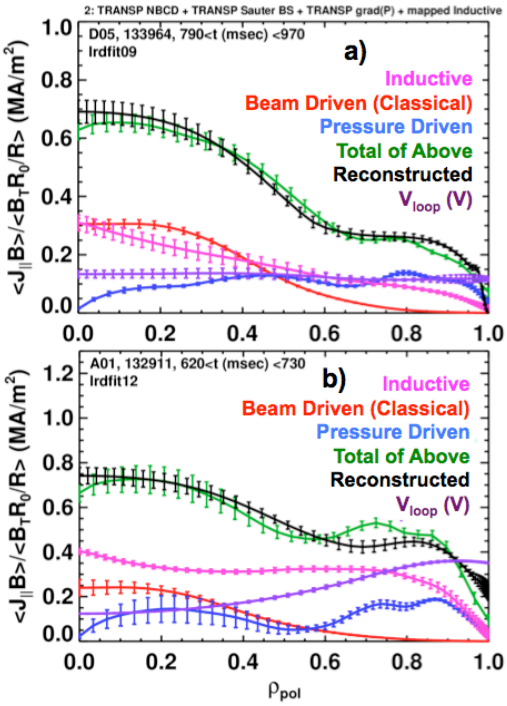

Fig. 5) Current profile reconstructions for discharges designed to maximize the a) non-inductive fraction, and b) the stored energy.

Figure 5 shows a detailed analysis of the current profile for high-performance plasmas at low and high current: a) an I_P=700 kA high-β_P plasma designed to maximize the non-inductive fraction, and b) an I_P=1300 kA plasma designed to maximize the stored energy. The bootstrap current is computed in TRANSP [17] using the Sauter model [18], and the neutral beam current is computed with the NUBEAM code [19]. The inductive current is determined by computing the loop voltage profile from a time-sequence of MSE constrained equilibria [20] and multiplying it by the neoclassical resistivity as computed in the Sauter

model. The measured carbon profile is the only impurity in the calculation. There is no low-frequency MHD during the chosen time windows, and no anomalous fast ion diffusion was used in either of these calculations; there is a good match between the measured and simulated neutron emission rates for these two cases.

Considering the lower current case in frame a) first, we see that the loop voltage profile is flat, indicating that the current profile has stopped evolving. The profile shows a characteristic two-hump shape, with the edge feature coming from the sum of bootstrap and inductive currents, and the core feature from the inductive and beam driven currents. Good agreement is found between the current profile inferred from MSE constrained reconstruction (black) and from summing the individual current constituents (green). Similar agreement is found in the high-current case in frame b). Note, however, that the loop voltage profile in this case is hollow, indicating that the current has not fully penetrated. Much more detailed analysis and discussion of the non-inductive current profile in NSTX high-performance plasmas can be found in Ref. [21], including a discussion of cases where MHD modes cause fast-ion redistribution, and an upper bound on the fast-ion diffusivity in MHD-quiescent regimes.

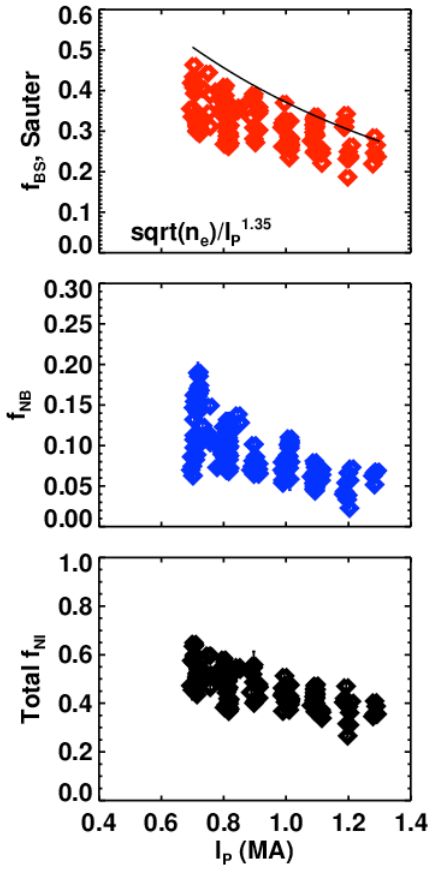

Fig. 6 Non-inductive current fractions vs. the plasma current.

Based on this success, we have run the TRANSP code for a large number of κ>2.3 H-mode plasmas, focussing on time windows where there is no low-frequency MHD activity. The database has a wide range of plasma currents (700 kA<I_P<1300 kA), toroidal fields (0.32<B_T (T)< 0.54), density (3.8×10^{13} < n_e (cm^{-3})< 9.5×10^{14}), power (2 < P_{inj} (MW)< 6), and elongation (2.3 < κ <2.8). Carbon is typically used as the only impurity, though a few cases use a flat Z_{eff} profile whose time dependence matches that from a visible bremsstrahlung measurement. No anomalous fast ion diffusion is used, and good matches between the measured and simulated stored energy and neutron emission have been verified. The time windows for averaging are 60-100 msec. long, and are at least ~1.5 current redistribution times past the start of the I_P flat-top. Error bars in this database come from the standard deviation of the signals within the averaging window.

The non-inductive current analysis from this database is shown in Fig. 6, where the data is plotted against the plasma current. The bootstrap fraction is shown in frame a), and unsurprisingly increases as the plasma current decreases. Using the $I_P^{0.65}$ scaling of energy confinements discussed below, we can see a scaling on the upper bound on the bootstrap fraction as $f_{BS} \propto \beta_P \sim \tau_E P / I_p^2 \sim \sqrt{n_e} / I_p^{1.35}$; this scaling is shown in frame a), and is in reasonable agreement with the data. The neutral beam current drive fraction in frame b) shows the expected decrease as I_P is increased. When the individual points are normalized to the injected beam power and volume averaged slowing down time, the points all fall on a $1/I_P$ curve. The total non-inductive fraction is shown in frame c), showing that 65-70% of the plasma current has been driven non-inductively at lower values of the plasma current. Future experiments at lower plasma current will test this trend, although bad-orbit losses of the fast ions may prove problematic at low I_P.

4. Transport in characteristics of high-performance plasmas

Designs for next-step ST devices typically assume that the confinement will meet or exceed the expectations from traditional H-mode scaling expressions like ITER-98 [14]. The large database of TRANSP runs utilized above is useful for providing information on this issue. In addition, dedicated scans of I_P and B_T in high-performance plasmas with lithium PFC conditioning have been analysed.

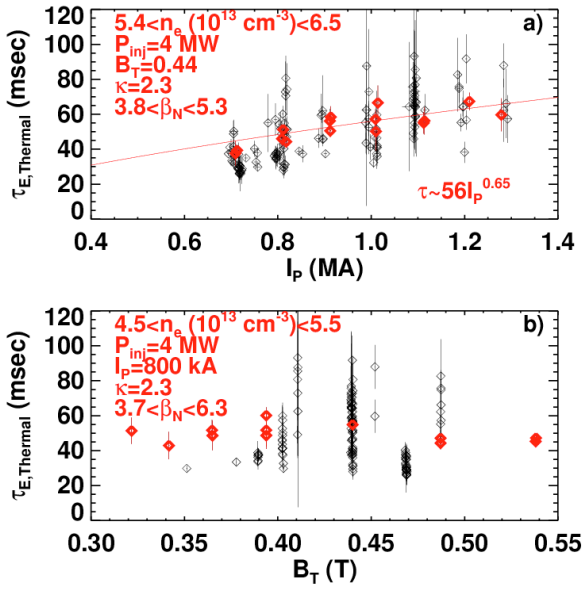

Fig. 7. a) I_P and b) B_T scaling of the thermal confinement time, for the large database (black), and controlled scans (red).

The global confinement scaling of confinement in these high-performance plasmas is somewhat different than that reported in previous studies in NSTX [22] and MAST [23]; the difference is likely due to the lithium conditioning of the plasma facing components (PFCs) in these recent plasmas. One important difference is the stronger I_P scaling in this data, compared to previous NSTX experiments that showed $\tau_{E,Thermal} \propto I_P^{0.4}$. This can be seen most clearly in Fig. 7a), where the thermal confinement time is plotted against the plasma current for the entire database in black, and for the devoted scan in red. A trend of increasing confinement with plasma current is observed in both cases, with the devoted scan indicating a dependence of $\tau_{E,Thermal} \propto I_P^{0.65}$. A more striking difference with previous results relates to the B_T dependence of confinement, as shown in Fig. 7b). Both the large database and devoted scan show that the scaling of $\tau_{E,Thermal}$ with B_T is weak or nonexistent under these conditions, unlike previous experiments that showed $\tau_{E,Thermal} \propto B_T^{0.9}$. The details regarding this clear change in confinement characteristics are under active investigation.

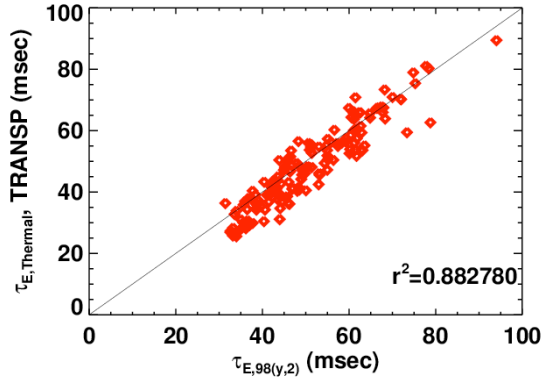

Fig. 8. Comparison of the measured thermal confinement time with ITER-98 scaling, for a database of high-performance H-modes.

The results presented in the previous paragraph show that the field and current dependence of thermal confinement in these discharges is similar to that in conventional aspect ratio H-mode tokamaks. This is confirmed by the data in Fig. 8, where the calculate confinement time is plotted against the expectation from the ITER-1998 H-mode scaling expression $\tau_{E,Thermal} \propto I_P^{0.93} B_T^{0.15} n_e^{0.41} P_{inj}^{-0.69}$. The agreement is found to be quite good over a large range of confinement times, though the NSTX data may on average be slightly beneath the scaling expectation. Note that the discharges in this dataset were chosen for their sustained high-β nature. Many discharges with better confinement may not be included, either because the confinement increase leads to a β-limit disruption, or because the good confinement is achieved without strong shaping and sustained high-β.

5. Stability properties

Beyond the strong shaping described in Fig.4, other tools are critical for progress in developing high performance plasmas. The control of resonant [12] and non-resonant [24] error fields, and feedback on the unstable resistive wall mode [25], are critical for maintaining the high-β state; the more recent progress in this area is summarized in [26]. Lithium conditioning of the PFCs broadens the pressure profile, improving the global stability [27]. A modification to the rtEFIT basis vectors has improved reconstructions critical to control.

An additional new tool is the realtime adjustment of the injected power to control the plasma β_N. The normalized β is calculated in realtime with rtEFIT code [28]. A PID operator is applied to the difference between the requested and achieved β_N, to calculate a new input power. The proportional and integral gains were determined using the Ziegler-Nichols tuning method: the delay, time-sale and magnitude of the β_N response to pre-programmed changes in the NB input power are used to determine values of the proportional and integral gains.

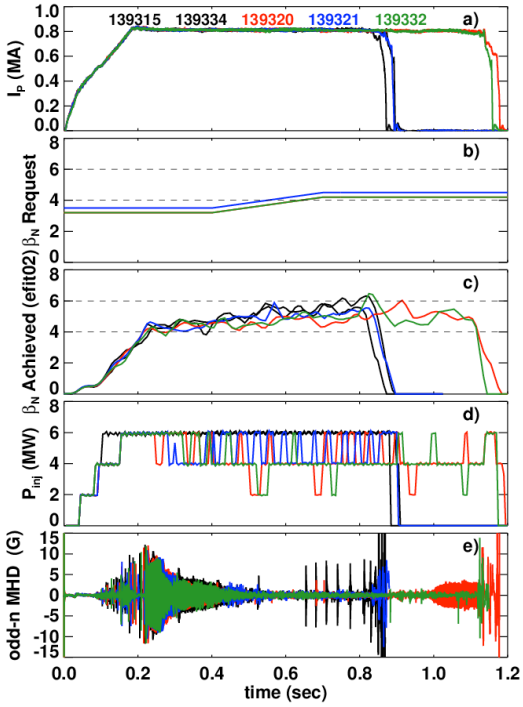

Fig. 9) Demonstration of β_N control in high-κ, high-β discharges.

An example use of this capability is shown in Fig. 9, where the target plasma is a κ=2.5 high performance scenario at 800 kA. The two black discharges are run with 6 MW of pre-programmed neutral beam power, and are seen to develop RWMs and disrupt at t=0.8 s. The green and red discharges were run with the β_N algorithm turned on at t=0.2 s. The β_N value is consequently somewhat lower, and the discharges are sustained for significantly longer. The red case develops a core n=1 modes that eventually locks to the vessel and disrupts, while the green case suffers from an H->L back-transition. The blue discharge also utilizes β_N control, but with a slightly higher β_N request. There is consequently more power provided to the discharge and a higher β_N value, and the discharge disrupts at nearly the same time as the 6MW references. This examples shows that the β_N controller can indeed improve higher-performance discharges, though a judicious β_N request is required. For instance, the ramp in the request was found to be necessary, as having the higher request early invariably lead to disruption. Note that this issue could be eliminated by feeding back on a more accurate estimate of proximity to a stability boundary, for instance, the plasma amplification of an applied n=1 field [29]. This new capability for β_N control has also been used in support of other experiments. For instance, it was utilized to maintain constant β_N during I_P and B_T scans associated with a tearing mode onset experiment; use of the algorithm to adjust the injected power minimized the number of discharges by eliminating the need the manually adjust the injected power waveform for each I_P and B_T combination.

Beyond the plasma shape, the profile shapes play an important role in determining the global stability. Broader pressure profiles improve the plasma global stability. Reducing the internal inductance tends to be destabilizing, with instability predicted at very low β_N for sufficiently low l_i. In order to explore this physics using the achieved NSTX shapes and profiles, the no-wall and with-wall β_N limit was calculated as a function of time for a number of high-

performance discharges. This calculation relied on reconstructions constrained by external magnetics, the magnetic pitch angle from MSE, the plasma diamagnetism, and the requirement that T_e be an isotherm. The CHEASE code [30] was then used to generate

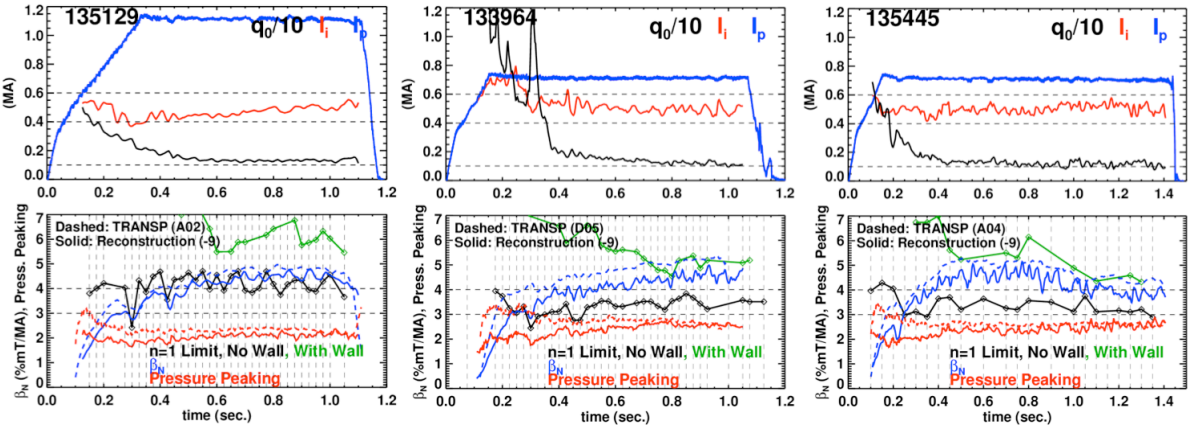

Fig. 10. Ideal stability analysis for a series of high-performance discharges. The plasma current, q_0 and internal inductance are shown in the top frames, while the bottom frames shows the calculated no-wall and with-wall n=1 stability limits, β_N value, and pressure peaking factor.

equilibria with a range of scaled pressure profiles and β_N values, keeping the profile shapes and plasma boundary unchanged. The DCON [31] code used to assess the global kink stability of each equilibrium and compute the no-wall & with-wall stability limits. Typically 30-40 CHEASE and DCON runs are used for each time-point.

A summary of this analysis is shown in Fig. 10, where three discharges are analyzed in detail. The internal inductance and q_0 come from equilibrium reconstructions, while the β_N and pressure peaking (central pressure normalized by the volume average pressure) are derived from both equilibrium reconstructions (solid) and TRANSP (dashed) calculations. The first column shows a high-κ 1100 kA discharge. The internal inductance is quite low, as is the pressure peaking: the net result is that the no-wall β_N limit of ~4.2 is quite comparable to that in lower performance discharges. The second and third columns show the calculation for the 700 kA high-β_P and long pulse discharge discussed above. The internal inductance stays low, but the pressure peaking is significantly higher than the 1100 kA case. This combination results in a significantly reduced no-wall limit of ~3.5. The ideal-wall limit in these cases decreases with time, and the experimental β_N value becomes comparable to ideal limit at the end of the shot. Detailed parametric studies of how these beta limits depend on these profile and shape parameters will be the subject of future research.

In addition to ideal instabilities like the RWM, core kink/tearing modes have been observed to deleteriously impact performance in these discharges. Reconstructions of these modes using the fluctuating ultra-soft X-ray emission and model eigenfunctions show that they are typically 2/1 magnetic islands [32] coupled to 1/1 core kink modes [21,33]. These modes reduce the plasma rotation and confinement, and often lock to the wall, leading to H-mode loss and disruption. These lithium-conditioned plasmas are typically free of ELMs, sawteeth, and other MHD perturbations that can trigger neoclassical islands. Recent work with the M3D code [34] has shown that the growth of non-resonant m/n =1/1 modes as q_0 nears 1 may be responsible for the onset of the observed coupled modes. The details of the onset, including why some discharges are able to maintain their high-β phase with q_0 near 1 for long periods, remains a topic of research.

The authors would like to thank the members of the neutral beam operations team for their help with the β_N feedback system, and the NSTX engineering and operations teams for

their support. This research was funded by the United States Department of Energy under contract DE-AC02-09CH11466. Prepared by LLNL under Contract DE-AC52-07NA27344.

References:

[1] Y.K.M. PENG and D.J. STRICKLER, Nuclear Fusion **26** (1986) 769.
[2] F. NAJMABADI and the ARIES Team, Fusion Eng. And Design **65** (2003) 143.
[3] H.R. WILSON, et al, Nuclear Fusion **44** (2004) 917.
[4] J. E. MENARD, et al, Nuclear Fusion **37** (1997) 595.
[5] R.L. MILLER, et al, Nuclear Fusion **4** (1997) 1062.
[6] R.J. GOLDSTON, et al, *An Experiment to Tame the Plasma Material Interface*, IAEA Fusion Energy Conference, Paper FT/P3-12, Geneva (2008).
[7] Y-K M PENG, et al., Plasma Phys. Control. Fusion **47** (2005) B263.
[8] H.R WILSON, et al., *A Steady State Spherical Tokamak for Components Testing*, IAEA Fusion Energy Conference, Paper FT/3-1Ra, Villamoura, Portugal (2004).
[9] G.M. VOSS, et al., Fusion Eng. and Design **83** (2008) 1648.
[10] M. ONO, et al, Nuclear Fusion **40** (2000) 557.
[11] J.E. MENARD, et al., Phys. Rev. Lett **97** (2006) 095002.
[12] J.E. MENARD, et al., Nuclear Fusion **50** (2010) 045008.
[13] D. A. GATES, et al., Nuclear Fusion 49, (2009) 104016.
[14] ITER PHYSICS EXPERT GROUPS, Nuclear Fusion **39** (1999) 2175.
[15] D. A. GATES, et al, Phys. Plasmas **13** (2006) 056122.
[16] E. LAZARUS, et al, Phys. Plasmas B **3** (1991) 2220.
[17] R. J. HAWRYLUK, et al., "An Empirical Approach to Tokamak Transport", in Physics of Plasmas Close to Thermonuclear Conditions, ed. by B. Coppi, et al., (CEC, Brussels, 1980), Vol. 1, pp. 19-46.
[18] O. SAUTER, C. ANGIONI, and Y.R. LIN-LIU, Phys. Plasmas **6** (1999), 2834.
[19] A. PANKIN et al, Comput. Phys. Commun. **159** (2004) 157.
[20] C.B. FORREST, et al, Phys. Rev. Lett. **73** (1994) 2444.
[21] S.P. GERHARDT, et al, *Calculation of the Non-Inductive Current Profile in High-Performance NSTX Plasmas,* submitted to Nuclear Fusion.
[22] S.M. KAYE, et al., Phys. Rev. Lett. **98** (2007) 175002.
[23] M. VALOVIC, et al, Nuclear Fusion **49** (2009) 075016.
[24] S.P. GERHARDT, et al., Plasma Phys. Control Fusion **52** (2010) 104003.
[25] S.A SABBAGH et al., Nuclear Fusion **50** (2010) 025020.
[26] S.A. SABBAGH, et al., *Resistive Wall Mode Stabilization and Plasma Rotation Damping Considerations for Maintaining High Beta Plasma Discharges in NSTX*, Paper EXS/5-5, Daejeon (2010).
[27] M. BELL et al, Plasma Phys Control Fusion **51** (2009) 124054.
[28] D.A. GATES, et al., Nuclear Fusion **46**, (2006) 17.
[29] H. REIMERDES et al., Nuclear Fusion **45** (2005) 368.
[30] H. LUTJENS, et al., Comp. Phys. Comm. **97**, 219 (1996).
[31] A. H. GLASSER and M.C. CHANCE 1997 *Bull. Am. Phys. Soc.* **42** 1848.
[32] S.P. GERHARDT, et al., Nuclear Fusion **49** (2009) 032003.
[33] J.E. MENARD, et al., Nuclear Fusion **45** (2005) 539.
[34] J. BRESLAU, et al, *Onset and Saturation of a Non-Resonant Internal Mode in NSTX and Implications for AT Modes in ITER*, Paper THS/P2-03, Daejeon (2010).